Characterisation of the Cyclic Deformation Behaviour of the Nodular Cast Iron ASTM 80-55-06 on the Basis of Physical Measurement Methods

Holger Germann[#1], Peter Starke[#2], Dietmar Eifler[#3]

[#]*Institute of Materials Science and Engineering;University of Kaiserslautern*
P.O. Box 3046, 67653 Kaiserslautern, Germany

[1]germann@mv.uni-kl.de
[2]starke@mv.uni-kl.de
[3]eifler@mv.uni-kl.de

***Abstract*—The current paper is focussed on the nodular cast iron ASTM 80-55-06 (EN-GJS-600). The individual microstructure was investigated by light and scanning electron microscopy as well as micro-hardness measurements. Stress-controlled fatigue tests were performed at ambient temperature with testing frequencies of f = 5 Hz and f = 150 Hz. The cyclic deformation behaviour was characterised by means of mechanical stress-strain hysteresis (f = 5 Hz) as well as the change in temperature, electrical resistance and frequency (f = 150 Hz) measurements. Increasing testing frequencies result in higher values of the change in temperature caused by the increasing heat dissipation per second.**

I. Introduction

Good mechanical, physical and manufacturing properties as well as the relatively low production costs lead to a common interest in cast irons for various technical applications [1]. Due to the combination of a relatively high tensile strength and an adequate ductility nodular cast iron is often used for highly stressed components in the automotive and commercial vehicle industry, e.g. for crankcases, crankshafts or exhaust manifolds, as well as in the wind power industry, e.g. for rotor hubs or nacelles [2-5]. An appropriate material selection and a weight-optimised dimensioning are essential for safe and economic operation conditions of such cast iron components. Therefore, the characterisation of the fatigue behaviour is of major importance. In the literature, fracture-mechanic investigations [6-8] as well as fatigue tests with mechanical stress-strain hysteresis [9] and in some cases temperature measurements [10] are described for nodular cast iron [11].

In the scope of the current paper stress-controlled fatigue tests were performed with specimens of the nodular cast iron ASTM 80-55-06 (EN-GJS-600) at ambient temperature on servohydraulic testing systems with a testing frequency of 5 Hz and on resonators with a testing frequency of 150 Hz. For a detailed microstructural-based characterisation of the fatigue behaviour, high-precision mechanical stress-strain hysteresis (f = 5 Hz), temperature, electrical resistance and frequency (f = 150 Hz) measurements were applied. The plastic strain amplitude ($\varepsilon_{a,p}$) as well as the change in temperature (ΔT), electrical resistance (ΔR) and frequency (Δf) were plotted versus the number of cycles in cyclic deformation, cyclic temperature, cyclic electrical resistance and cyclic frequency curves. All measured quantities are based on microstructural changes due to fatigue processes in the plastically deformed volume of the gauge length of the specimens, e.g. deformation-induced matrix debonding of the graphite. On the basis of the measured temperature data a linear relation between the ΔT values at f = 5 Hz and f = 150 Hz was found. For both testing frequencies the Woehler (S-N) curves were determined. In addition, fracture surfaces were investigated by using scanning electron microscopy (SEM).

II. Investigated Cast Iron

The cast iron ASTM 80-55-06 (EN-GJS-600) was provided by the Daimler AG in round bars with a diameter of 36 mm and a length of 300 mm. Brinell hardness measurements yield values of 235±6 HBW30. Figure 1 shows characteristic light (a) and scanning electron (b) micrographs of the investigated material. The microstructure consists of a pearlitic matrix with a ferrite content of 14.6±2 area-% and a graphite content of 9.8±0.8 area-%. As can be seen in Figure 1, the formation of ferrite is predominantly observed in ferrite zones located in the surrounding of the graphite nodules. The mean diameter of the graphite nodules was determined to 19.1±6.8 µm. Table I summarises the microstructural parameters of the cast iron.

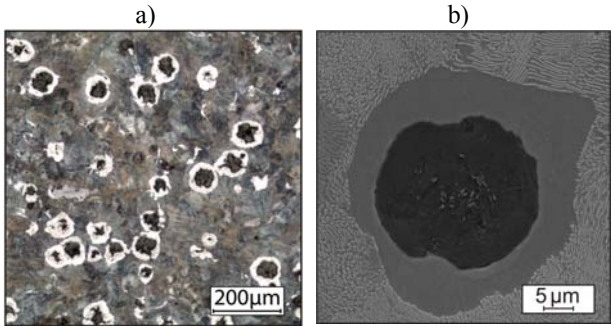

Fig. 1 Light (a) and scanning electron (b) micrographs of the microstructure of the cast iron ASTM 80-55-06 (**EN-GJS-600)**

TABLE I
MICROSTRUCTURAL PARAMETERS OF THE CAST IRON ASTM 80-55-06
(EN-GJS-600)

Ferrite fraction [area-%]	Graphite fraction [area-%]	Mean diameter of nodules [µm]
14.6±2	9.8±0.8	19.1±6.8

In order to evaluate the hardness of the pearlite, ferrite and graphite fraction a Martens micro-hardness pattern with a width of 200 x 200 µm was measured on a polished cross-section (Figure 2). The load of 0.1 N was applied without a hold time within 10 s. Afterwards, the microstructure was etched and correlated with the results of the micro-hardness measurements. The micro-hardness values significantly decrease in the sequence pearlite (3095 HM0.1), ferrite (1757 HM0.1) and graphite (597 HM0.1). Corresponding to the phase distribution, a mean micro-hardness value of 2654 HM0.1 can be calculated by multiplying the pearlite (ferrite, graphite) content with the appropriate micro-hardness value of 3095 (1757, 597) HM0.1. It is possible to revalue the Martens hardness to Vickers hardness and a revaluation according to [12] yields about 240 HV0.1. This value shows a good accordance with the Brinell hardness determined to be 235±6 HBW30.

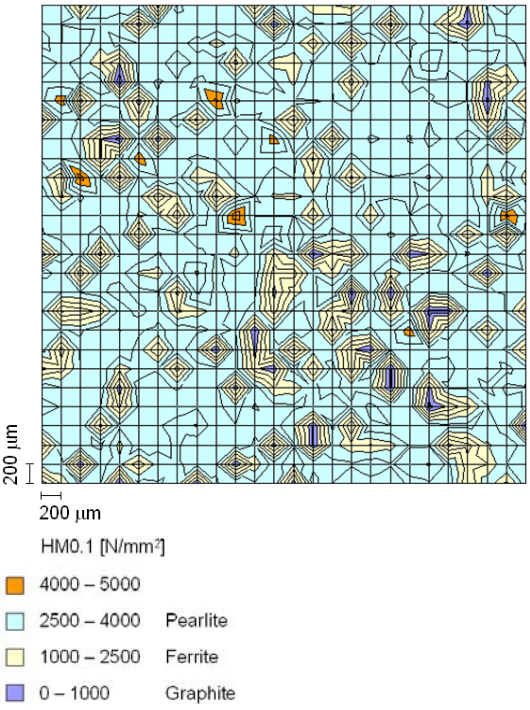

Fig. 2 Martens micro-hardness pattern for the cast iron ASTM 80-55-06 **(EN-GJS-600)**

All fatigue tests were performed with the specimen geometry shown in Figure 3.

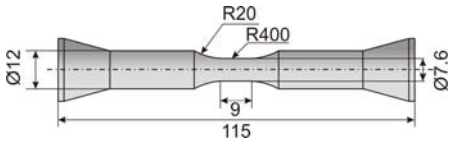

Fig. 3 Specimen geometry

III. EXPERIMENTAL SETUP

Stress-controlled load increase tests (LITs) and constant amplitude tests (CATs) were carried out at ambient temperature at a testing frequency of 5 Hz on servohydraulic testing systems using a triangular load-time function at a load ratio of R = -1. In the LITs, the stress amplitude σ_a was increased from $\sigma_{a,\,start}$ continuously with the rate $d\sigma_a/dt = 11.1 \cdot 10^{-3}$ MPa/s until specimen failure. The CATs were performed until failure or to a maximum number of cycles N_{max} of $2 \cdot 10^6$. In Figure 4, the experimental setup is shown schematically.

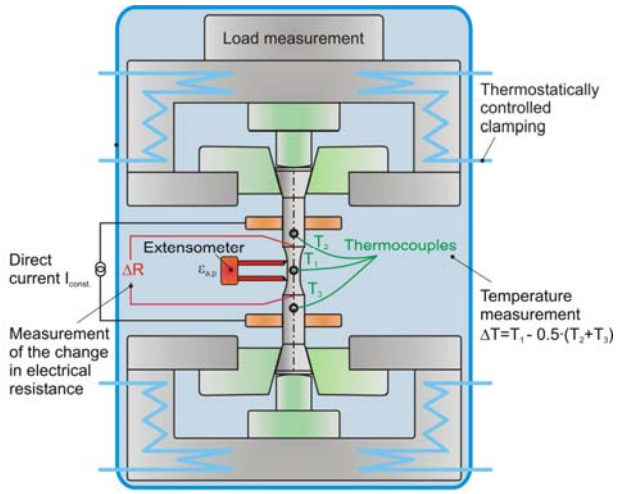

Fig. 4 Experimental setup for mechanical hysteresis, temperature, and electrical resistance measurements during fatigue loading schematically

During the fatigue tests, the plastic strain amplitude $\varepsilon_{a,p}$ [13], the change in temperature ΔT [14] and the change in electrical resistance ΔR [15] were measured to characterise the microstructure-based fatigue behaviour in detail. The physical quantities $\varepsilon_{a,p}$, ΔT and ΔR are a function of the deformation induced change in microstructure in the bulk of the specimen and represent the actual fatigue state [16-19]. For the measurement of $\varepsilon_{a,p}$ an extensometer was fixed in the middle of the gauge length. The change in temperature ΔT was detected with one thermocouple in the middle of the gauge length (T_1) and two thermocouples at the elastically loaded specimen shafts (T_2 and T_3). For electrical resistance measurements a DC-power supply was fixed at both shafts and ΔR was measured with two wires spot welded at the transition of the gauge length and the shafts (Figure 4). Apart from the geometry, the change in electrical resistance ΔR strongly depends on the resistivity ρ^* which is directly related to deformation induced changes in the microstructure, e.g. dislocation density and arrangement, vacancies, micro-

pinholes, micro-shrinkage cavities or micro-cracks. In the case of cast irons the measured value ΔR is of major importance, in particular to get detailed information about the actual fatigue state with respect to damage mechanisms like graphite-matrix debonding.

Furthermore, stress-controlled CATs were performed at ambient temperature at a testing frequency of 150 Hz on a resonator using a sinusoidal load-time function at a load ratio of R = -1 until specimen failure or to a maximum number of cycles N_{max} of $2 \cdot 10^7$. In addition to the above mentioned physical quantities, the change in frequency Δf of the electromagnetical resonance device can be used for the characterisation of the fatigue behaviour. Caused by the functional principle of a resonator the specimen is part of the spring-mass-system of the testing setup and the measured value Δf depends on the damping behaviour of the specimen which depends on the deformation induced changes in the microstructure during fatigue loading [20].

IV. Results

A. Load Increase Tests

Load increase tests (LITs) allow a reliable estimation of the endurance limit with one single specimen related to a maximum number of cycles $N_{max} = 2 \cdot 10^6$. In Figure 5, besides the stress amplitude σ_a, the plastic strain amplitude $\varepsilon_{a,p}$, the change in temperature ΔT and the change in electrical resistance ΔR are plotted versus the number of cycles N for a LIT with the cast iron ASTM 80-55-06 (EN-GJS-600). The ΔR-N curve indicates an initial decrease, among others caused by closing micro-cracks during the compression half cycles. Then, the courses of the change in electrical resistance ΔR are characterised by a saturation state between $6 \cdot 10^4$ and $1 \cdot 10^5$ cycles, followed by an increase indicating cumulative graphite-matrix debonding and micro-crack growth. A significant change in the slope of the $\varepsilon_{a,p}$-N, ΔT-N and ΔR-N curve of the LIT occurs at $\sigma_{RW,\,LIT} = 220$ MPa. This stress amplitude can be used for the estimation of the endurance limit [14]. The stress amplitude 398 MPa leads to specimen failure.

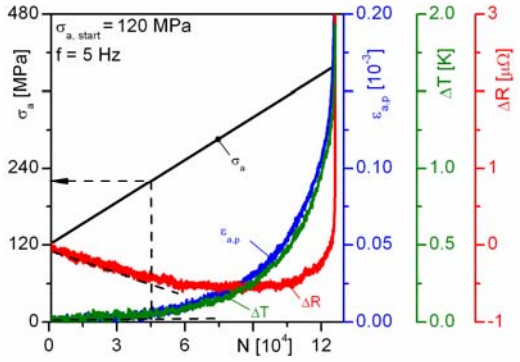

Fig. 5 Plastic strain amplitude, change in temperature and change in electrical resistance in a continuous load increase test for the cast iron ASTM 80-55-06 **(EN-GJS-600)**

B. Constant Amplitude Tests

Constant amplitude tests (CATs) were performed with stress amplitudes in the range of $220 \leq \sigma_a \leq 340$ MPa at a testing frequency of 5 Hz. In Figure 6a, the plastic strain amplitude is plotted versus the numbers of cycles. The $\varepsilon_{a,p}$-N curves immediately indicate plastic strain amplitudes between $0.015 \cdot 10^{-3}$ for $\sigma_a = 220$ MPa and $0.12 \cdot 10^{-3}$ for $\sigma_a = 340$ MPa followed by cyclic hardening processes in the matrix until macroscopic crack growth. After an initial increase caused by thermal conduction, the ΔT-N curves shown in Figure 6b also describe the cyclic hardening as a consequence of reduced plastic deformation. In Figure 6c, the change in electrical resistance is plotted versus the numbers of cycles. At first, the ΔR-N curves are characterised by a decrease leading to minimum ΔR values between -2.81 μΩ for $\sigma_a = 220$ MPa and -1.32 μΩ for $\sigma_a = 340$ MPa. Then, with increasing numbers of cycles an enforced graphite-matrix debonding and micro-crack growth result in increasing ΔR-N values.

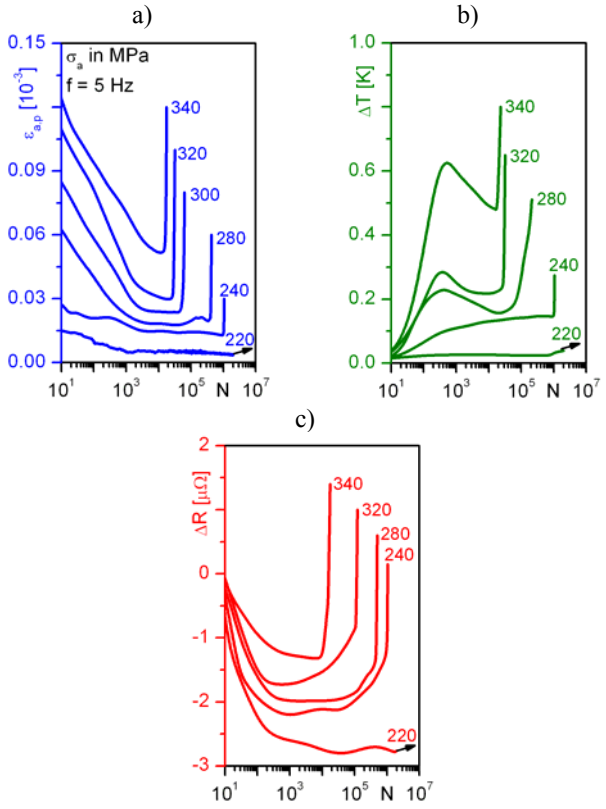

Fig. 6 Cyclic deformation curves (a), cyclic temperature curves (b) and cyclic electrical resistance curves (c) for constant amplitude tests with a testing frequency of 5 Hz for the cast iron ASTM 80-55-06 **(EN-GJS-600)**

The CATs performed with stress amplitudes in the range $240 \leq \sigma_a \leq 340$ MPa lead to numbers of cycles to failure between $2 \cdot 10^4$ and $1 \cdot 10^6$ whereas the CAT performed with $\sigma_a = 220$ MPa reaches $2 \cdot 10^6$ cycles without failure. The stress amplitude of 220 MPa corresponds very well to $\sigma_{RW,\,LIT} = 220$ MPa estimated in the LIT. This underlines the high capability of LITs for a reliable estimation of the

endurance limit of cast irons with one single specimen. Thus, this test procedure yields large economic advantages.

To evaluate the influence of the testing frequency on the cyclic deformation behaviour, CATs were performed in the range of $190 \leq \sigma_a \leq 280$ MPa at a starting testing frequency of 150 Hz. In Figure 7, cyclic deformation curves are shown on the basis of the change in temperature ΔT (a) and the change in frequency Δf (b). The ΔT-N curves are characterised by an initial increase due to thermal conduction leading to maximum ΔT values which are located between 1.12 K for $\sigma_a = 190$ MPa and 5.48 K for $\sigma_a = 280$ MPa. Then, a decrease of the ΔT-N curves indicates cyclic hardening processes in the matrix until macroscopic crack growth. The change in frequency depends on the before mentioned cyclic deformation behaviour of the investigated material, whereby a decrease (increase) of the Δf values is caused by an increase (decrease) of the damping capacity. At first, a slight increase of the Δf values probably indicating micro-crack closure occurs. Then, with increasing numbers of cycles the Δf-N curves decrease due to a cumulative graphite-matrix debonding and micro-crack growth. The CATs performed with stress amplitudes in the range $200 \leq \sigma_a \leq 280$ MPa result in numbers of cycles to failure between $3.5 \cdot 10^5$ and $3.5 \cdot 10^6$. The CAT performed with $\sigma_a = 190$ MPa reaches $2 \cdot 10^7$ cycles without failure.

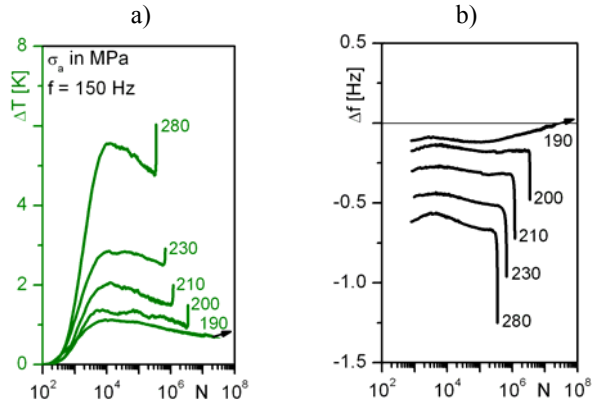

Fig. 7 Cyclic temperature curves (a) and cyclic frequency curves (b)) for constant amplitude tests with a testing frequency of 150 Hz at the range $190 \leq \sigma_a \leq 280$ MPa for the cast iron ASTM 80-55-06 **(EN-GJS-600)**

In Figure 8, the change in frequency Δf is plotted as a function of the change in temperature ΔT at $N = 1 \cdot 10^4$ cycles at stress amplitudes in the range $190 \leq \sigma_a \leq 280$ MPa. As can be seen, there is a linear relation between both quantities.

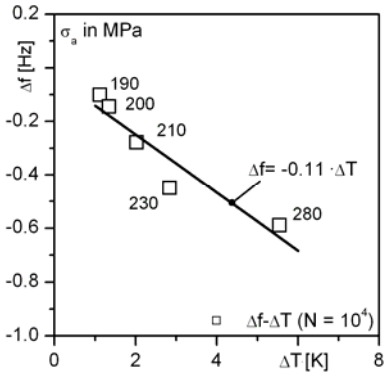

Fig. 8 Linear relation between the change in frequency and the change in temperature for f = 150 Hz for the cast iron ASTM 80-55-06 **(EN-GJS-600)**

Figure 9 shows the comparison of the ΔT-N curves for constant amplitude loading with $\sigma_a = 280$ MPa at the testing frequencies of 5 Hz and 150 Hz. An increase in the testing frequency from f = 5 Hz to f = 150 Hz leads to significantly higher ΔT values because of a higher heat dissipation per second in the plastically deformed gauge length of the specimen.

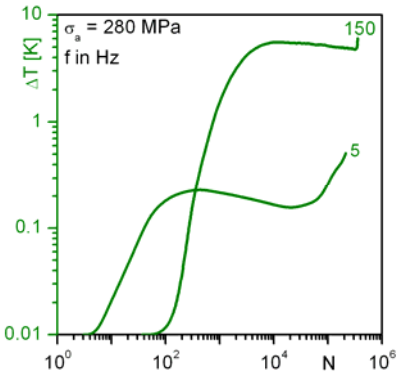

Fig. 9 Comparison of the cyclic temperature curves at f = 5 Hz and f = 150 Hz for constant amplitude loading with $\sigma_a = 280$ MPa for the cast iron ASTM 80-55-06 **(EN-GJS-600)**

At stress amplitudes of 220 MPa, 230 MPa and 280 MPa CATs were performed at testing frequencies of 5 Hz and 150 Hz. On the basis of temperature data measured at $1 \cdot 10^4$ cycles a linear relation between the ΔT values for f = 5 Hz $\Delta T_{5\,Hz}$ and the ΔT values for f = 150 Hz $\Delta T_{150\,Hz}$ can be calculated. The $\Delta T_{5\,Hz}$-$\Delta T_{150\,Hz}$ relation is presented in Figure 10. The ratio $\Delta T_{5\,Hz}/\Delta T_{150\,Hz}$ determined to 0.039 corresponds very well with the ratio between the testing frequencies of 0.033. This illustrates that a higher testing frequency results in higher heat dissipation per second and unit of the plastically deformed volume in the gauge length of the specimen. The increase of the temperature is a function of decreasing values of the plastic strain amplitude [22,23] and the increased heat dissipation per second for increasing testing frequencies.

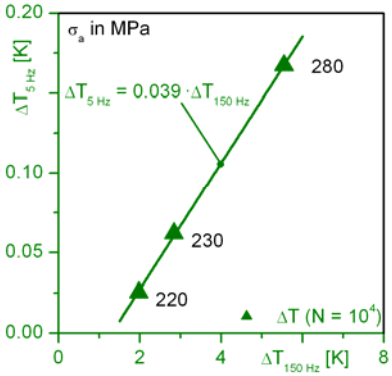

Fig. 10 Linear $\Delta T_{5\,Hz}$-$\Delta T_{150\,Hz}$ relation determined on the basis of temperature data measured at $1 \cdot 10^4$ cycles in constant amplitude tests with a frequency of f = 5 Hz and f = 150 Hz for the cast iron ASTM 80-55-06 **(EN-GJS-600)**

Figure 11 shows the Woehler (S-N) curves for both testing frequencies. As can be seen e.g. in [22], provided that the testing conditions are identical, an increase in the testing frequency generally results in longer lifetimes. Nevertheless, with regard to the CATs performed in the scope of this paper, due to the different load-time functions, at identical stress amplitudes the lifetimes are slightly longer at f = 5 Hz (triangular load-time function) in comparison to f = 150 Hz (sinusoidal load-time function), see e.g. [23]. The endurance limit was not determined statistically in the scope of this paper. At f = 5 Hz (f = 150 Hz) the specimen loaded with 230 MPa (190 MPa) reaches $2 \cdot 10^6$ ($2 \cdot 10^7$) cycles without failure.

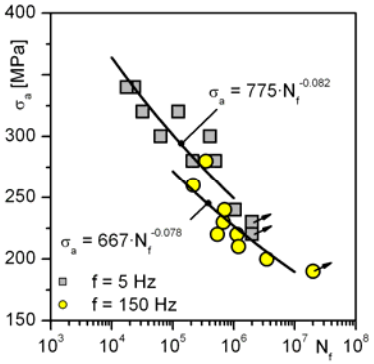

Fig. 11 Woehler curves for the testing frequency f = 5 Hz and f = 150 Hz for the cast iron ASTM 80-55-06 **(EN-GJS-600)**

To get more information about the fracture mechanisms fracture surfaces were investigated with scanning electron microscopy (SEM). Independent of the stress amplitude and the testing frequency the initiation of fatigue cracks can be often observed at defects, like micro-pinholes or micro-shrinkage cavities. Figure 12a shows the fatigue crack initiation at a defect in the centre of the fracture surface of a specimen, which was loaded with $\sigma_a = 300$ MPa at a testing frequency of 5 Hz and reached a number of cycles to failure of $4.1 \cdot 10^5$. In Figure 12b, the striation area is shown in detail. The final fracture surface, which is shown in Figure 12c in detail, is characterised by characteristic dimple structures.

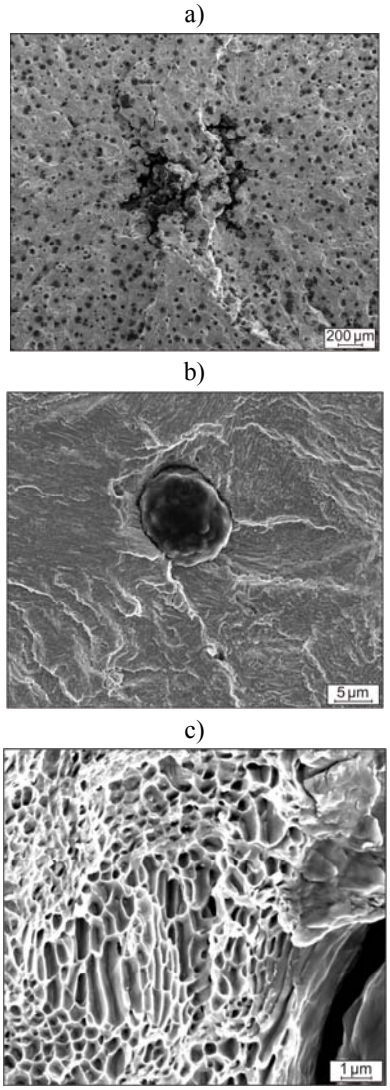

Fig. 12 Crack initiation at a defect in the centre of the specimen (a), striation area (b) and final fracture surface (c) for a constant amplitude test with $\sigma_a = 300$ MPa at a testing frequency of 5 Hz for the cast iron ASTM 80-55-06 **(EN-GJS-600)**

V. Summary

The present paper is focused on the cast iron ASTM 80-55-06 (EN-GJS-600). The microstructure predominantly consists of a pearlitic matrix with nodular graphite. In load increase tests at a testing frequency of 5 Hz the endurance limit of the investigated cast iron can be estimated with one single specimen. The cyclic deformation behaviour under constant amplitude loading was characterised at the testing frequencies f = 5 Hz and f = 150 Hz on the basis of the plastic strain amplitude (f=5Hz) as well as the change in temperature, electrical resistance and frequency (f=150 Hz). At both testing frequencies the cyclic deformation behaviour is dominated by cyclic hardening of the matrix and graphite-matrix debonding until macroscopic crack initiation. In the constant amplitude tests at f = 150 Hz higher values for the change in temperature were measured caused by the higher energy dissipation per

second in the plastically deformed gauge length compared to fatigue tests with f = 5 Hz. With respect to the change in temperature ΔT, a liner relation between the ΔT values at f = 150 Hz and f = 5 Hz can be determined. The fatigue strength at f = 5 Hz is slightly higher than at f = 150 Hz because of the different load time functions, in particular triangular for f = 5 Hz and sinusoidal for f = 150 Hz.

ACKNOWLEDGMENT

The support of the German Research Foundation (Deutsche Forschungsgemeinschaft) is gratefully acknowledged.

REFERENCES

[1] R. O'Rourke, "Cast iron: The engineered metal," *Advanced Materials & Processes*, vol. 159, pp. 65-68, Jan. 2001.

[2] M Hafiz, "Mechanical properties of SG-iron with different matrix structure," *Journal of Materials Science*, vol. 36, pp. 1293-1300, 2001.

[3] M. A. Kenawy, A. M. Abdel-Fattah, N. Okasha and M. EL-Gazery, "Mechanical and Structural Properties of Ductile Cast Iron," *Egyptian Journal of Solids*, vol. 24, pp. 151-159, 2001.

[4] F. Iacoviello, O. Di Bartolomeo, V. Di Cocco and V. Piacente, "Damaging micromechanisms in ferritic-pearlitic ductile cast irons," *Materials Science and Engineering A* , vol. 478, pp. 181-186, 2008.

[5] D. Veldkamp, "A probabilistic evaluation of wind turbine fatigue design rules," *Wind Energy*, vol. 11, pp. 655-672, 2008.

[6] T. Ogawa and H. Kobayashi, "Near threshold fatigue crack growth and crack closure in a nodular cast iron," *Fatigue & Fracture of Engineering Materials & Structures*, vol. 10, pp. 273-280, 1987.

[7] H. Yaacoub Agha, A.-S. Béranger, R. Billardon, and F. Hild, "High-cycle fatigue behaviour of spheroidal graphite cast iron," *Fatigue & Fracture of Engineering Materials & Structures*, vol. 21, pp. 287-296, 1997.

[8] P. Hübner, H. Schlosser, G. Pusch, and H. Biermann, "Load history effects in ductile cast iron for wind turbine components," *International Journal of Fatigue*, vol. 29, pp. 1788-1796, 2007.

[9] C. Guillemer-Neel, V. Bobet, and M. Clavel, "Cyclic deformation behaviour and Bauschinger effect in ductile cast iron," *Materials Science and Engineering A, vol.* 272, pp. 431-442, 1999.

[10] H. Q. Xue, E. Bayraktar, and C. Bathias, "Damage mechanism of a nodular cast iron under the very high cycle fatigue regime," *Journal of Materials Processing Technology*, vol. 202, pp. 216-223, 2008.

[11] P. Hübner, G. Pusch and L. Krodel, "Fatigue Behaviour of Cast iron with Globular Graphite," *Advanced Engineering Materials*, vol. 6, pp. 541-544, 2004.

[12] C. Heermant and D. Dengel, "Klassische Werkstoffkennwerte abschätzen," *MP Material Testing*, vol. 38, pp. 374-378, 1996.

[13] P. Lukáš and M. Klesnil, "Cyclic stress-strain response and fatigue life of metals in low amplitude region," *Materials Science and Engineering*, vol. 11, pp. 345-356, 1973.

[14] D. Dengel, H. Harig, "Estimation of the fatigue limit by progressively increasing load tests," *Fatigue & Fracture of Engineering Materials & Structures*, vol. 3, pp. 113-128, 1980.

[15] J. Polák, "Electrical resistivity of cyclically deformed copper," *Czechoslovak Journal of Physics*, vol. 18, pp. 315-322, 1969.

[16] P. Starke, F. Walther, and D. Eifler, "PHYBAL – A new method for lifetime prediction based on strain, temperature and resistance measurements," *International Journal of Fatigue*, vol. 28, pp. 1028-1036, 2006.

[17] P. Starke, F. Walther, and D. Eifler; "Fatigue assessment and fatigue life calculation of quenched and tempered SAE 4140 steel based on stress-strain hysteresis, temperature and electrical resistance measurements," *Fatigue & Fracture of Engineering Materials & Structures*, vol. 30, pp. 1044-1051, 2007.

[18] P. Starke and D. Eifler, "Fatigue assessment and fatigue life calculation of metals on the basis of mechanical hysteresis, temperature, and resistance Data," *MP Materials Testing*, vol. 51, pp. 261-268, 2009.

[19] H. Germann, P. Starke, E. Kerscher, and D. Eifler, "Fatigue behaviour and lifetime calculation of the cast irons EN-GJL-250, EN-GJS-600 and EN-GJV-400," *Procedia Engineering*, vol. 2, pp. 1087-1094, 2010.

[20] V. Wagner, P. Starke, E. Kerscher, and D. Eifler, „Cyclic deformation behaviour of railway wheel steels in the very high cycle fatigue (VHCF) regime," *International Journal of Fatigue*, vol. 33, pp. 69-74, Jan. 2011.

[21] D. Eifler, *Zusammenhang zwischen Mikrostruktur und Schwingfestigkeitsverhalten bei Stählen*, D. Munz, Ed.. Oberursel, Germany: DGM Informationsgesellschaft mbH, 1985.

[22] W. J. Harris, Ed., *Metallic Fatigue*, ser. International Series of Monographs in Aeronautics and Astronautics, Division VIII: Materials Science & Engineering. Oxford, United Kingdom: Pergamon Press, 1961, vol. 1.

[23] K. Koibuchi and M. Yamane, "Wave-form effect on fatigue strength and its rheological analysis", *Bulletin of JSME*, vol. 11, pp.761-770, 1968.